I. – LONG RANGE ORDER – EXTENDED DEFECTS – NON STOICHIOMETRY.ELECTRON MICROSCOPY POTENTIALITIES FOR THE STUDY OF PHASE TRANSITIONS IN SOLIDS

J. van Landuyt

ELECTRON MICROSCOPY POTENTIALITIES FOR THE STUDY OF PHASE TRANSITIONS IN SOLIDS

J. VAN LANDUYT

Rijksuniversitair Centrum Antwerpen, Middelheimlaan 1, B-2020 Antwerpen, Belgium

Résumé. — Les possibilités de la microscopie et de la diffraction électronique pour la détection et l'analyse des processus ordre-désordre et autres transitions de phase dans les solides sont résumées.

En particulier on discute la relation des défauts structuraux et les transformations des types : cisaillement, cisaillement cristallographique, ordre-désordre et *displacive*.

L'étude des transformations par les images de leurs défauts aussi bien que par les changements dans les diffractions est discutée et illustrée par l'analyse de quelques études particulières choisies parmi différents types de transitions comme : les transformations par cisaillement entre deux polytypes de TaS_2, les transformations ordre-désordre dans la structure spinelle lacunaire de β-In_2S_3 et la transition *displacive* entre les phases α et β du quartz.

Abstract. — A survey is given of the potentialities of electron microscopy and electron diffraction for the detection and analysis of order-disorder processes and phase transitions in solids.

Particular attention is paid to the relation with crystallographic defects of respectively shear, crystallographic shear, order-disorder and displacive transformations.

The study of transformations by their related effects in the transmitted image as well as by changes in the diffraction pattern will be discussed and illustrated by the analysis of a few case studies chosen among different types of transitions such as the shear transition between TaS_2-polytypes, the order-disorder transitions in the defective spinel structure of β-In_2S_3 and the displacive $\alpha \rightarrow \beta$ phase transition in quartz.

Introduction. — Electron microscopy, in particular transmission electron microscopy coupled with electron diffraction, have become a very valuable tool to study order-disorder transformations and phase transitions in general.

Thanks to its imaging facilities, defects associated with the transformations can be visualised ; moreover the electron diffraction data of the same areas allow the detection of order or any other changes in structural symmetry.

The combination of both often yields valuable information on the structure defects and their role in the transformation mechanism. The usefulness of the technique is to be found in particular on the microstructural scale where domain boundaries and twins often severely inhibit X-ray diffraction analysis.

In a first general chapter we shall relate the characteristics of phase transitions with the aspects that are observable by electron microscopy and diffraction. Thereafter we shall by the analysis of some particular case studies illustrate the potentialities of the technique.

1. **Direct information on the ordering process.** — If a phase transition occurs in a temperature range between — 120 °C and 800° to 900 °C any commercial electron microscope equiped with the now available heating and cooling stages can be used to obtain direct information on phase transitions.

1.1 DIFFRACTION EVIDENCE. — The diffraction pattern even of a very small area will reveal characteristic changes since at the transition temperature usually changes in symmetry with or without an associated lattice deformation do occur. The disorder to order transition being usually accompanied by a decrease in symmetry is often revealed by the addition of superlattice spots in particular positions determined by the structural relation between ordered and disordered phase. A simple example is illustrated for a (111)-pattern of a b.c.c. solid solution of gaseous impurities in niobium which upon ordering gives rise to *superlattice spots* at half distance between the 110-reflections (figure 1) [1]. The intensity of the superlattice spots is proportional to $S^2(f_A - f_{A'})^2$ where S is the degree of ordering and f_A, $f_{A'}$, are the atomic scattering factors. The intensity thus depends on the difference in scattering factor between the ordering species and the degree of order. The comparatively very large scattering power of electrons ($10^4 \times f_x$) makes electron diffraction particularly

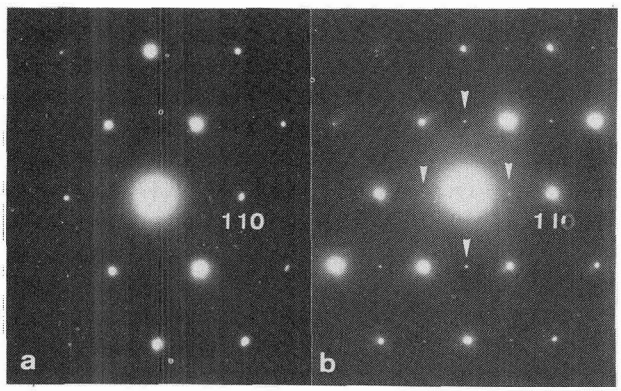

FIG. 1. — (111)-patterns in niobium with gaseous impurities in solid solution. If the interstitials are ordered additional spots are observed (*b*).

useful for detecting order even in very small domains or nuclei.

Another example is illustrated in figure 2 where three clearly distinct diffraction patterns are associated with two intrapolytypic phase transitions in a 1T-TaS_2 crystal.

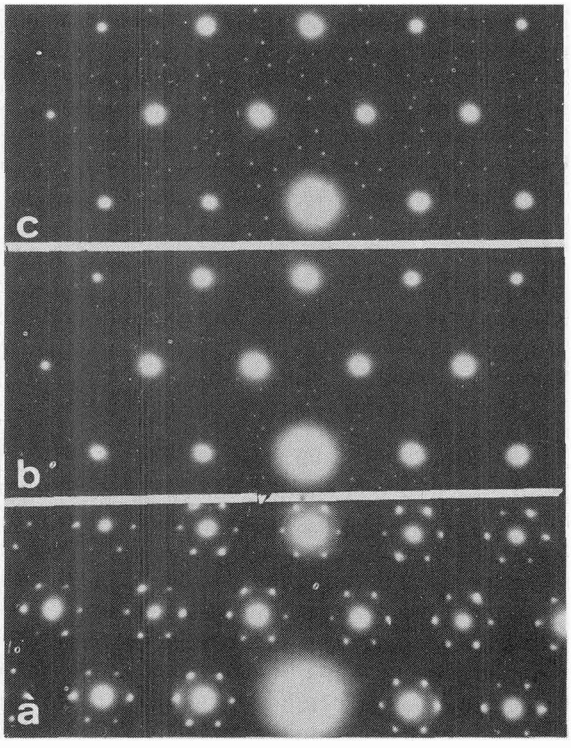

FIG. 2. — Changes in a basal section pattern of 1T-TaS_2 as a consequence of intrapolytypic transition. Notice the incommensurability of the patterns.

Often also *diffuse intensity* in diffraction patterns is indicative of short range order or a transition state, and valuable information on the ordering mechanism can be obtained from a systematic analysis of the locus of these intensity maxima (in this symposium a contribution by R. De Ridder, D. Van Dyck, G. Van Tendeloo and S. Amelinckx will deal extensively with this matter). A typical example is illustrated in figure 3 [2].

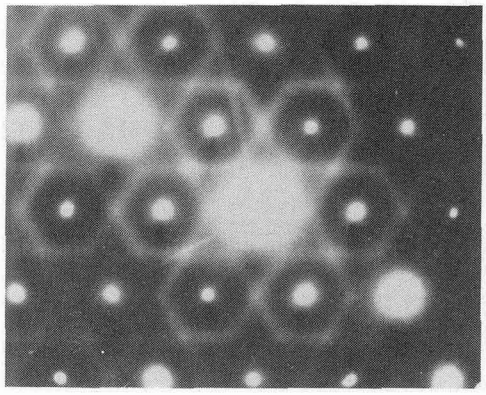

FIG. 3. — Diffuse scattering in copper intercalated NbS_2. Note the absence of diffuse scattering around spots of type $11\bar{2}0$ and around the origin.

A third diffraction effect whereby the presence of order can some-times be revealed even if the direction of ordering is unfavorable for the observation of superlattice spots, is associated with the lattice deformation that often accompanies ordering. Since the deformation may be small the effect is best observed on the higher order reflections, and is particularly evident if ordering twins are included in the selected area as in the example in figure 4 where the spot splitting is clearly seen.

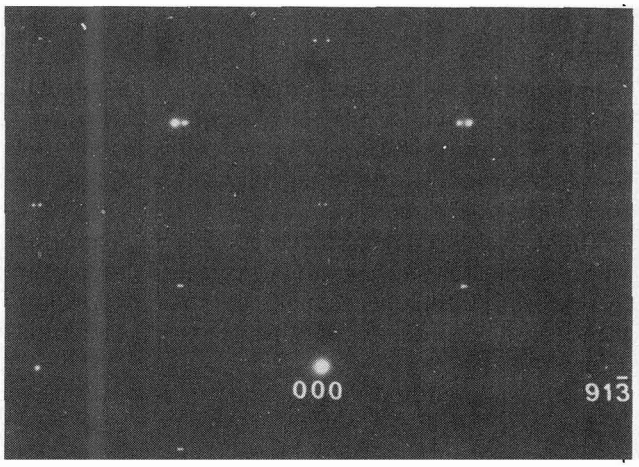

FIG. 4. — Spot splitting due to the presence of two orientation variants. This splitting is associated with order induced deformation.

In conclusion of this paragraph we can attribute the power of electron diffraction for detecting order to its high sensitivity and the possibility offered in electron microscopes to select very small areas for diffraction in order to reveal and disentangle data from even very small ordering domains.

The possibility to observe these changes *in situ* enables the determination of the transition tempera-

ture. Also certain aspects of the nature of the transition such as the appearance of a pretransitional state or intermediate phases are revealed in diffraction.

1.2 EVIDENCE FROM THE DIRECT IMAGE OBSERVATION OF THE TRANSFORMATION MECHANISM. — In some cases where direct observations can be made *at* the transition temperature, the electron beam can be used to produce a temperature gradient across the observed area. Depending on the type of transition the transformation mechanism can directly be visualized either as

— growing nuclei or plates
— passage of a discontinuous front
— passage of a complex configuration of defects
— the transition occurring e.g. shear transformation by dislocation passage.

An example of each is illustrated in figures 5, 6, 7 and 8. Figure 5 illustrates the nucleation and growth of an ordered interstitial solid solution in niobium [3]. A discontinuous front between the γ and β 1T-TaS_2 phase is shown in figure 6 [4], whereas figure 7 reveals a complex front consisting of a nearly regular network of Dauphiné twins at the phase transition from $\alpha \rightarrow \beta$ quartz [5]. A shear transformation in progress is illustrated by the dislocation configurations in TaS_2 in figure 8 [6].

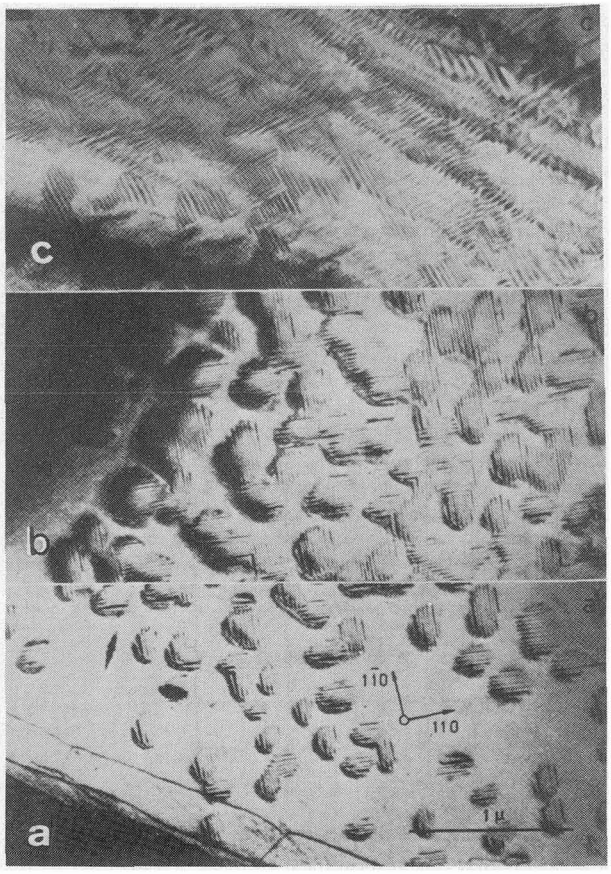

FIG. 5*abc*. — Subsequent stages of a nucleation process of order of interstitials in niobium. In (*a*) isolated nuclei are formed composed of small parallel platelets in ⟨ 110 ⟩ directions of the (100) plane. The nuclei grow together until they touch (*b*), to form the cross-hatched pattern in (*c*).

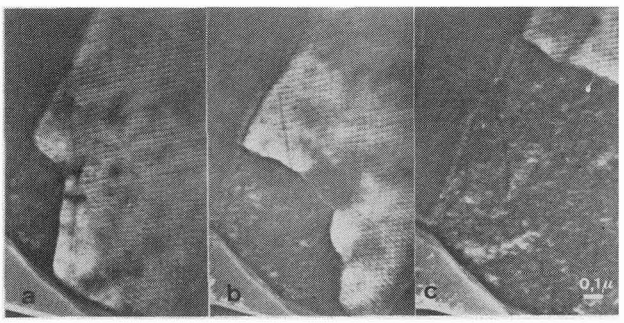

FIG. 6. — Dark field images revealing a discontinuous transformation front between the β and γ-phases of 1T-TaS_2.

2. **Indirect information.** — Apart from the direct information which is often, for what the transmitted images is concerned, hampered by a reduced resolution due to the experimental circumstances (heating, cooling) a lot of information can also be obtained from post transformation observations. It is clear that there equally well the diffraction evidence can be used to detect and analyse phases either in an equilibrium or a quenched-in state.

In particular I want to deal in this paragraph with the indirect evidence gained from the observation and analysis of *lattice defects* associated with the transformations. Often these defects play an important role in the transition itself such as the dislocations in a shear transformation or sometimes they are secondary consequences of it such as twins to accommodate strain, or antiphase boundaries originating from the coalescence of domains.

Phase transformations are almost invariably accompanied by changes in symmetry. A reduction in symmetry occurs in going from the high temperature to the low temperature phase or from the disordered to the ordered phase. This reduction in symmetry results in the formation of a *domain structure* because the lower symmetry structure can be formed from the higher one in a number of crystallographically equivalent ways. A typical example of a domain structure resulting from the reduction of symmetry at a transition is shown in figure 9 for niobiumditelluride. The number of variants can be deduced from simple group theoretical considerations [8] which can answer questions such as :

— the number of different translation interfaces
— the number of different orientation variants
— the relative orientation of these variants
— the number of different interfaces between these variants.

Transmission electron microscopy allows us to observe these variants directly by the diffraction contrast they produce. We will primarily discuss the two dimensional defects which are of major importance in order disorder processes.

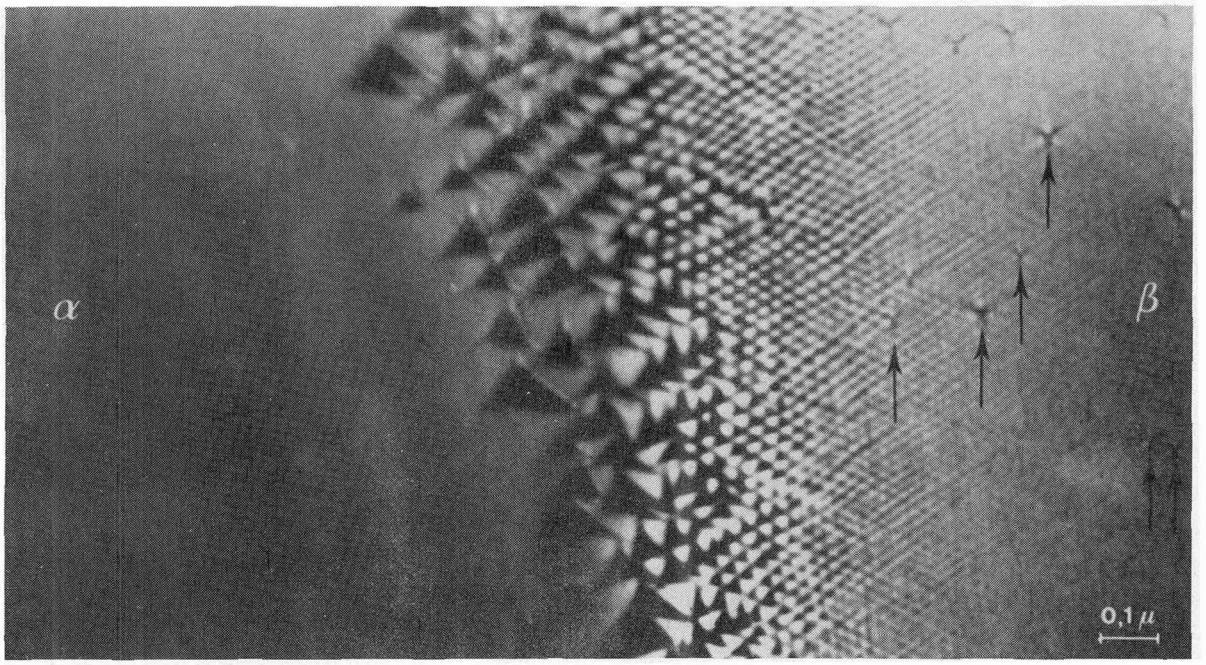

FIG. 7. — Complex transition *front* composed of regular arrays of dauphiné twins in quartz. To the left the crystal is in the α-phase, to the right in the β-phase.

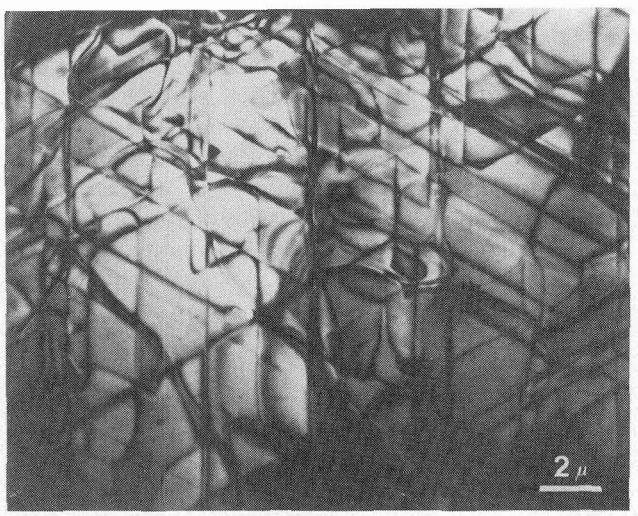

FIG. 8. — Transformation dislocations associated with the 1T → 2H transition in TaS_2. Note the triangular figures and the wavy dislocation lines.

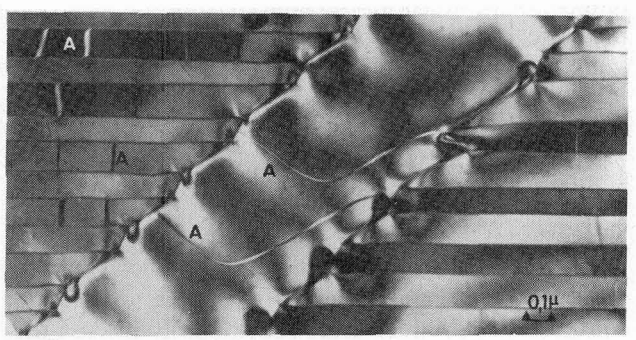

FIG. 9. — Domain configuration in $NbTe_2$. Translation (A) as well as orientation variants are observed.

Schematically a *translation interface* in an ordered structure can be represented as in figure 10 and is usually called an antiphase boundary (APB). The origin of APB's is easily imagined as the interface between two crystal areas where ordering occurred in the same direction but started in non-equivalent sites. It is characterized by a displacement vector **R**, and depending on the orientation of this vector with respect to the interface the boundary is conservative or non-conservative (figure 11). Crystallographic shear planes are typical examples of non-conservative translation interfaces which play an important role in the formation of homologous oxide series.

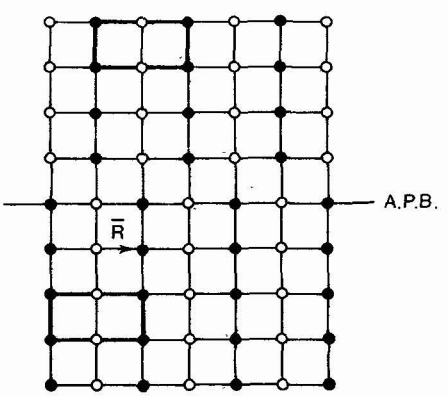

FIG. 10. — Translation variant in hypothetical two dimensional crystal. The displacement vector is indicated.

We shall not go into the details of contrast calculations involving dynamical diffraction theory, but will refer to the results of these calculations summa-

rized in table I [9]. The most general observation geometry is considered whereby the two dimensional defect is inclined with respect to the electron beam. A fringe pattern is then observed, the fringes being parallel with defect-crystal surface intersection lines. For antiphase boundaries and translation interfaces in general a fringe pattern is expected of the so-called α-type. α refers to the phase factor $\alpha = 2\pi\mathbf{gR}$ which determines the contrast for a reflection $\mathbf{g}$ of a translation interface with displacement vector $\mathbf{R}$. α-type fringe patterns are symmetrical in the bright field image and asymmetrical in the dark field image.

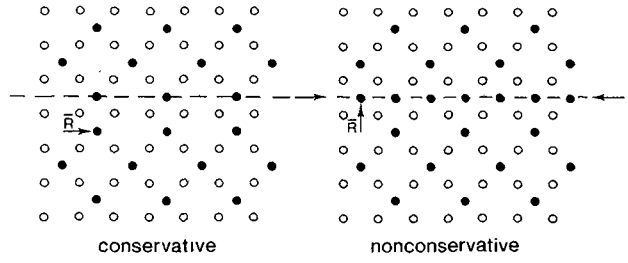

FIG. 11. — Conservative (*a*) and non-conservative (*b*) translation interface. A high density of interfaces as (*b*) allows to accommodate deviations from stoichiometry.

TABLE I

Type of interface	Image contrast effect	Extinction criterium	Diffraction pattern
1. antiphase boundaries (also shear planes) $\mathbf{R}$ = lattice vector of basic lattice but *not* of superlattice)	— imaged as α-fringes — no intensity difference between domains — visible in superlattice reflections only — long depth period	— $\mathbf{g}.\mathbf{R} = 0$ or integer — no contrast for fundamental	— no effect (apart from fine structure)
2. stacking faults $\mathbf{R}$ = not lattice vector	— images as α-fringes — no contrast difference between both parts — visible in fundamental reflections — small depth period	— $\mathbf{g}.\mathbf{R} = 0$ or integer	— no effect (apart from fine structure)
3. inversion boundaries	— interface images as α-type fringes — intensity difference between domains only in DF, and for certain multiple beam situations	— no contrast in BF — no contrast in DF if $\mathbf{g}$ belongs to a zone producing in projection a centre of symmetrie	— no effect (apart from possible fine structure)
4. domain boundaries $\mathbf{R}$ = displacement field $= kz^{\tau}$ (z = distance from interface) (k = small constant) (τ = twinning vector)	— δ fringes at interface — intensity difference in domains for most reflections — images by fundamental reflections — depth period is small ; may be different on both ends	— $\delta = 0$ for imaging reflections $\mathbf{g}.\mathbf{R} = 0$ in general	— if Δg is large enough spot splitting at high order spots (in fact superposition of two slightly different patterns) — all reflections are simultaneously excited in two parts
5. twins $\mathbf{R} = kz^{\tau}$ (z = distance from interface) (k = large constant) (τ = twinning vector)	— one part only is diffracting in general — interface imaged by thickness fringes	— $\mathbf{g}.\mathbf{R} = 0$; i.e. no contrast when imaged with common reflection	— one row of common reflections (unsplit spots) perpendicular to the twin plane — other spots are split parallel to row of unsplit spots — amount the splitting increases with distance from unsplit row in fact superposition of two diffraction patterns.

Antiphase boundaries are usually only revealed in superlattice reflections. The structure factor for these reflections is often rather small and consequently the extinction distance large. Since the latter determines the fringe spacing often only a limited number of fringes constitute the pattern.

The interface is out of contrast for a $\mathbf{g}$ vector for which $\alpha = 0$. A search of different so-called *extinctions* yields components of $\mathbf{R}$ and enables to determine it.

If a transition results in a non-centrosymmetric structure, interfaces between domains may originate which have an inversion relation with respect to each other. These have been termed *inversion boundaries*. A hypothetical example is illustrated in figure 12. The contrast characteristics are : in the BF image an α-type fringe pattern whereas dark field *multiple beam* images reveal a pronounced background intensity difference between both sides of the defect.

In the class of the orientation variants related to phase transitions we mainly have to mention the *ordering twins*. These result if different parts of the disordered phase the ordered structure is formed in

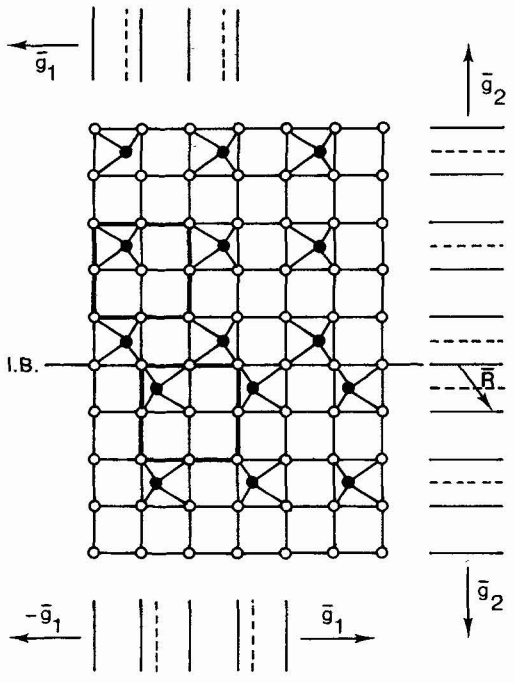

FIG. 12. — Two-dimensional model for an inversion boundary in a non-centrosymmetrical crystal. The boundary can be revealed by using reflections such as $\mathbf{g}_1$, but not by using reflections such as $\mathbf{g}_2$.

different but crystallographically equivalent directions (figure 13). Depending on the magnitude of the twinning vector the interfaces are termed *domain boundaries*, evidenced by δ-fringe patterns or twins revealed by wedge fringes. δ-fringe patterns are related with the orientation change by the parameter

$$\delta = s_1 t_1 - s_2 t_2 .$$

s_1, s_2 and t_1, t_2 are the excitation errors, respectively extinction distances for crystal parts 1 and 2 on either side of the boundary. The fringe patterns are now

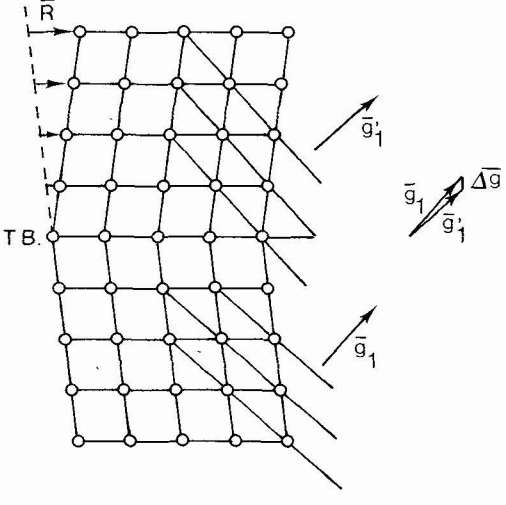

FIG. 13. — Twin configuration at orientation variant resulting from the deformation associated with the ordering.

asymmetrical in the bright field image and symmetrical in the dark field image. Contrary to antiphase boundaries here usually a background intensity difference is observed between both parts of the twin. The orientation variants are often most clearly evidenced in dark field images taken in the ordering spots where the respective variants are observed to *light-up* in the appropriate reflections.

The planar defects (stacking faults, shearplanes, antiphase boundaries, twins) sometimes occur in periodic arrays as it is the case for polytypes, mixed layer compounds, shear structures, superlattices and polysynthetic twin structures. If the period of these defects is sufficiently large the diffraction spots associated with it are necessarily included in the objective aperture, and the corresponding images directly reveal the periodicity of the defects.

Apart from the usual imaging conditions whereby the planar defect is inclined with respect to the incident electron beam, discussed in the previous pages and giving rise to fringe contrast, it is more interesting now to image the defects in geometries where they are exactly parallel with the electron beam.

In the case of single defects the image is a fine line as one could expect from the crude extrapolation of a fringe pattern. The theoretical analysis of the contrast is quite complicated and is not the subject of this contribution. Experimentally usually a fine dark line is observed as evidenced in figure 14 which shows both types of imaging conditions in one picture for shear planes in rutile.

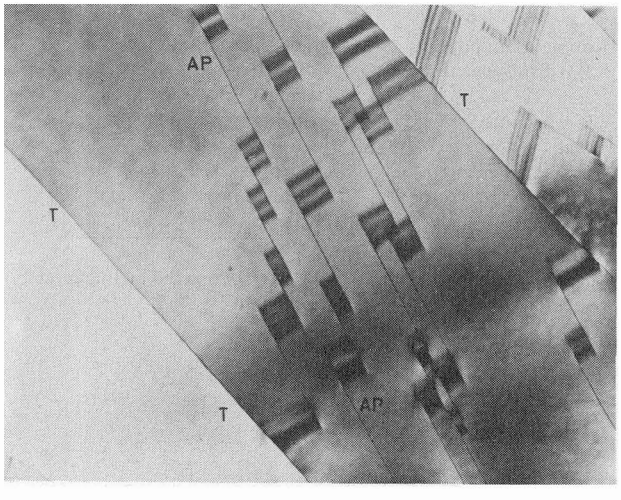

FIG. 14. — Antiphase boundaries in rutile. One family is parallel with the electron beam and observed as a fine line, the other family is inclined and observed as a fringe pattern. T are twins parallel with the beam.

2.1 OBSERVABLES AND INFORMATION EXTRACTED FROM THEM. — The contrast analysis of the defects, revealing their nature, and the crystallographic information such as habit plane, displacement vector, twin law that can be deduced from the associated

diffraction patterns often allow to propose a detailed model for the transition that has caused them.

First of all the *nature of the defects* can be deduced by making use of the image characteristics as summarized in table I from which it is clear that translation defects are easily distinguished from orientation defects. Stacking faults can be distinguished from antiphase boundaries by noting that stacking faults produce fringe contrast for certain fundamental reflections, but are out of contrast for all superlattice reflections. On the other hand antiphase boundaries produce fringe patterns for certain superlattice reflections and are out of contrast for all fundamental reflections.

It was already mentioned how the *displacement vector* can be deduced from extinction criteria. The knowledge of this vector is often useful in proposing a crystallographic model for the structural changes which are causing its existence. Another method for determining this displacement vector is appropriate for periodic arrays of translation interfaces, giving rise to diffraction effects due to the superperiod; here the diffraction pattern can be used to determine **R** in the following way [10].

The diffraction pattern due to the periodic arrangement of translation interfaces with a displacement vector **R** and a spacing d, is described by the relation

$$\mathbf{g} = \mathbf{H} + (1/d)\,(m - \mathbf{H}.\mathbf{R})\,\mathbf{e}_u$$

where $\mathbf{e}_u$ is the unit vector perpendicular to the interfaces; **g** and **H** are the diffraction vectors, respectively of the superlattice and of the lattice; m is an integer (figure 15). The diffraction pattern thus

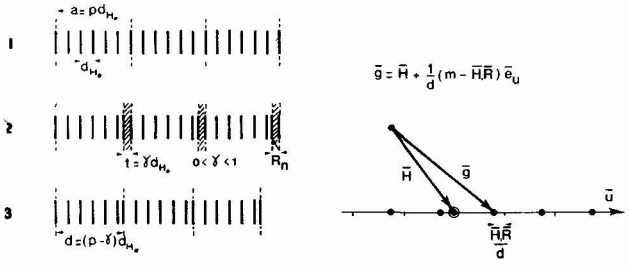

FIG. 15. — Schematic representation : effect on the diffraction pattern of a crystal containing a periodic array of non-conservative translation interfaces.

consists of linear arrays of superlattice spots **g**, grouped around each of the basic spots **H**, and shifted with respect to the basic spots by a fraction **H.R** of the interspot distance. A diffraction pattern from a selected area containing as well faultes as unfaulted structure thus allows to determine the projection of **R** on different **H** vectors (i.e. **H.R**). Two independent sections of reciprocal space are then sufficient to determine **R**. This method was applied to TiO_2, Ni_3Mo, Al_5Mo and γ-bras [11, 12, 13, 14].

From the knowledge of the **R** vector in the case of periodic non-conservative defects a structure model can be proposed from which the *local compositional difference* from that of the basic compound can be predicted. X-ray microanalysis in the electron microscope also allows to compare the composition of the areas with periodic faults with that of perfect material by measuring the ratios of the characteristic X-ray peaks in both areas. A typical application is illustrated in figure 16 where a region of Ni_3Mo is observed together with an area of quasi periodically arranged non-conservative antiphase boundaries. Whereas from the structural model and the displacement vector a composition of $Ni_{17}Mo_5$ was predicted, the microanalysis yielded a value of $Ni_{3.35}Mo$; the two values are apparently in very good agreement [12].

The combined use of diffraction evidence and contrast experiments often proves a powerful tool to analyse *domain structures.*

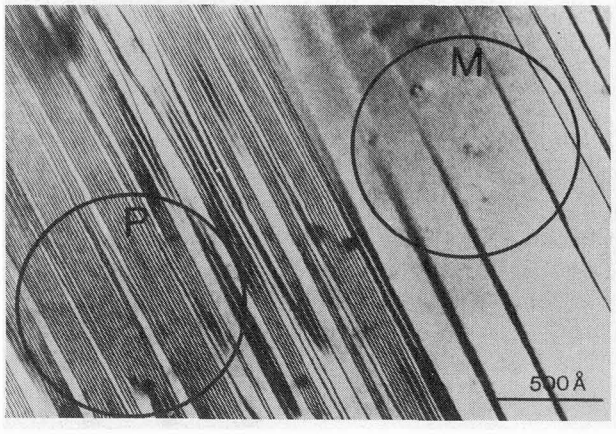

FIG. 16. — Region of Ni_3Mo containing quasi periodic faults together with perfect material from which the local composition can be measured.

If for certain diffraction conditions the background intensity in bright and dark field images is different in the domains on either side of the boundary one concludes that the interface has twin character. Also spot splitting is usually apparent, especially for the spots far from the centre.

Orientation variants resulting from ordering reactions usually give rise to diffraction patterns, which are a superposition of the patterns corresponding to the two variants, as it is the case for a regular twin. These patterns contain common spots which in the case of ordering domains coincide with the matrix spots. Making dark field images in one of these spots no contrast is revealed between the domains or twins; however in dark field images in one of the spots of the subpattern the corresponding variant lights up above the dark background resulting in a pronounced domain contrast. This procedure provides an excellent means to unravel the domain structure and its usually complex diffraction pattern.

3. **Case studies.** — The usefulness of the aforementioned techniques will now be illustrated by the

analysis of a few case studies. Only the essentials for the present purpose will be stressed. More information will be found in the original papers [6, 5, 15].

We will treat three different types of phase transitions :

1. The shear transformation 1T → 2H TaS_2.
2. The displacive phase transition $\alpha \rightarrow \beta$ SiO_2.
3. The order-disorder transitions in β-In_2S_3.

3.1 THE SHEAR TRANSFORMATION FROM 1T TO 2H-TaS_2 [6]. — The transition between polytypes such as 1T and 2H of tantalum disulphide can only take place by a shear transformation i.e. a mechanism whereby layers are displaced with respect to each other in an orderly way whereby a new structure is formed.

This transformation could directly be followed in the electron microscope since its temperature is within easy reach of the heating stage.

3.1.1 *Structural data.* — The 1-T phase has the cadmium iodide structure illustrated in figure 17*a*. This structure can be represented by the stacking symbol :

$$a\gamma b\ a\gamma b\ a\gamma b \ldots$$

where the latin letters represent the two positions for a close packed sulfur layer and the greek letters the positions of the tantalum close packed layers.

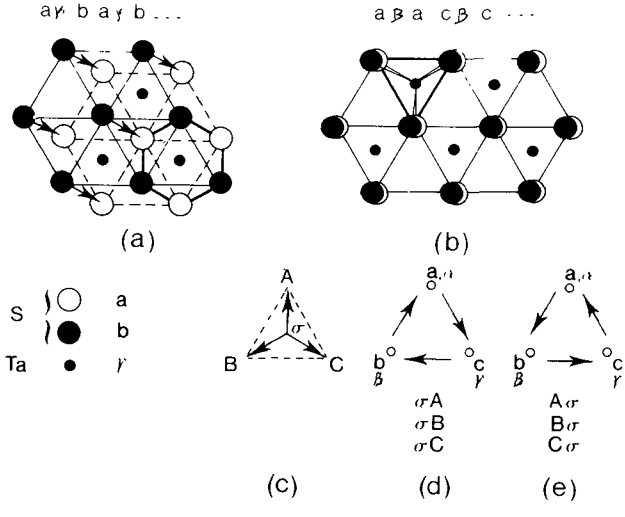

FIG. 17. — Structure of the 1T-TaS_2 (*a*) and the 2H (*b*) polytype. The stacking symbols are noted above each figure. In the lower part the symbols are shown as well as the dislocation nomenclature

The 2H-phase represented in figure 7*b* has the molybdenum disulphide structure. The stacking symbol is :

$$a\beta a\ c\beta c\ a\beta a\ c\beta c \ldots$$

It is clear from these structure projections that the transition between these phases can only occur by shifting of layers e.g. in the direction of the arrows indicated on figure 17*a*.

This can only occur by the passage of dislocations with a suitable burgersvector transforming the octahedral configuration of anions into a prismatic one.

The transformation dislocations need then to have a burgersvector of the same type as that of the Shockley partials, i.e. $\overline{\sigma A}$, $\overline{\sigma B}$ or $\overline{\sigma C}$ (figure 17*c*) but a glide plane, which in 2/3 of the cases has to be located between an anion and a cation layer, and in 1/3 of the cases between two sulfur layers. Normal glide dislocations have glide planes located between two anion layers, where the bonding is weakest.

The phase transformation can be performed by the passage of a transformation dislocation on the average every two layers. The passage of such a dislocation causes the stacking symbol to be changed according to the scheme shown in table II which represents symbolically the process.

It turns out that the passage of two transformation dislocations with burgersvector of the type $\overline{\sigma A}$, $\overline{\sigma B}$ or $\overline{\sigma C}$ (referred to in figure 17*c*) performing the shears (1) and (2) followed by the passage of an ordinary Shockley partial with the same burgersvector causing the shear (3) are needed.

The transformation process thus clearly needs two types of dislocations, with the same burgersvector, but a different type of glide plane. The shears need of course not to occur in a perfectly regular sequence as represented in table II, but in reality the transformation may proceed by means of dislocations, nucleated at random levels, usually along the foil edges, sometimes also in the centre of the foil.

TABLE II

$$\begin{array}{rl} & a|\gamma b\ \ a\gamma b\ \ a\gamma b\ \ a\gamma b\ \ a\gamma b \ldots \\ (1)| & \beta a\ \ c\beta|a\ \ c\beta a\ \ c\beta a\ \ c\beta a \ldots \\ (2) & \quad\ c\ |b\alpha c\ \ b\alpha c\ \ b\alpha c \ldots \\ (3) & \quad\ \ |a\gamma b\ \ a\gamma b\ \ a\gamma b \ldots \\ \ldots & a\beta a\ \ c\beta c\ \ a\gamma b\ \ a\gamma b\ \ a\gamma b \ldots \end{array}$$

2H 1T

3.1.2 *Observations.* — These layer crystals have inherently the *c*-plane as foil plane, the crystals are accordingly observed along an axis perpendicular to the drawing in figure 17. They were mounted in a heating stage and particular attention was paid to the temperature range about 297 °C where the 1T → 2H is due to take place. It was observed that on approaching the transformation temperature sufficiently slowly single individual dislocations can be seen to move along the basal plane, often as straight lines, parallel to the [$1\bar{1}20$] directions, giving rise to triangular shapes, as is visible in figure 8. There is mostly only a weak interaction between these straight transformation dislocations and the pre-existing glide dislocations in

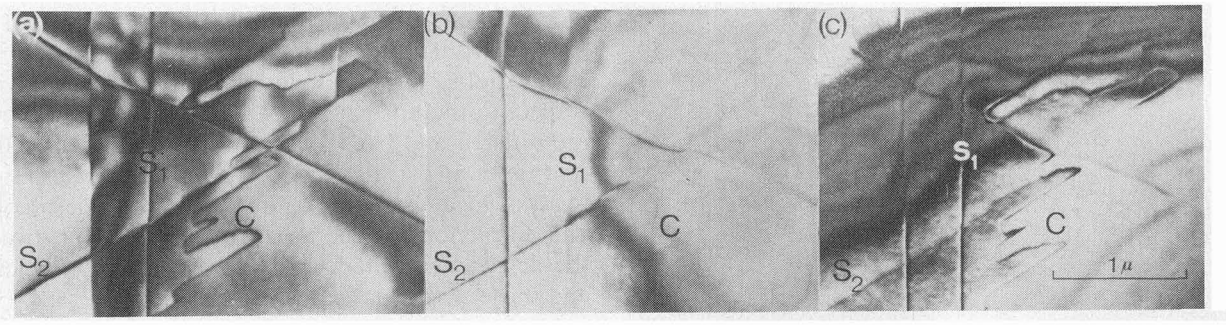

FIG. 18. — Different contrast situations for the same dislocation configuration in a partially transformed area : (*a*) Both types of dislocations in contrast. (*b*) One set of straight transformation dislocations (S_1) out of contrast together with the curvilinear dislocations (C) for a second hexagon type reflection. (*c*) A different set of straight dislocation lines (S_2) out of contrast for another { $11\bar{2}0$ } type reflection.

the basal plane, which remain mostly stationary during the transformation. Other moving dislocations participating in the transformation are more flexible and adopt arbitrary shapes during their movement. Both types of dislocations often leave a contrasted region behind under the proper imaging conditions, at least at the beginning of the transformation process, suggesting that they generate stacking faults. Whereas the transformation dislocations are single, the pre-existing glide dislocations consist of narrow ribbons at room temperature. An early stage where individual dislocations are observed is shown in figure 18*abc*. By contrast analysis of such configurations the two different types of dislocations could be distinguished, and their geometrical aspects, resp. rectilinear or curved could be related with their nature, resp. transformation dislocations (S_1, S_2) or Shockley partials (C).

3.2 THE $\alpha \rightarrow \beta$ PHASE TRANSITION IN QUARTZ : A DISPLACIVE TRANSITION [5]. — Quartz is well known to undergo a phase transition at 573 °C from low quartz α-phase to the high quartz β-phase. Although this transition has been studied often and by many different techniques the actual physical process was not unambiguously characterised. We therefore hoped that electron microscopy could shed some light on the process by direct observation at the transition temperature. The specimens were heated in the heating specimen holder and a gradient was produced by local heating with the electron beam.

3.2.1 *Structural data.* — α-quartz is hexagonal and belongs to the pointgroup 32 whereas β-quartz belongs to pointgroup 62. The loss in symmetry is clear from the projection along the *c*-axis in figure 19. Both the α and the β-structures are represented, and the α-phase is represented in its two variants α_1 and α_2. The structure consists of interlinked SiO_4 tetrahedra which are projected as trapezia in the α-phase and as squares in the β-phase. The relationship between the α_1 and α_2 variants is that of a rotation twin with the *c*-axis as twin axis : the dauphiné relationship.

3.2.2 *Observations.* — Close to the transition a large number of defects is observed. These defects are

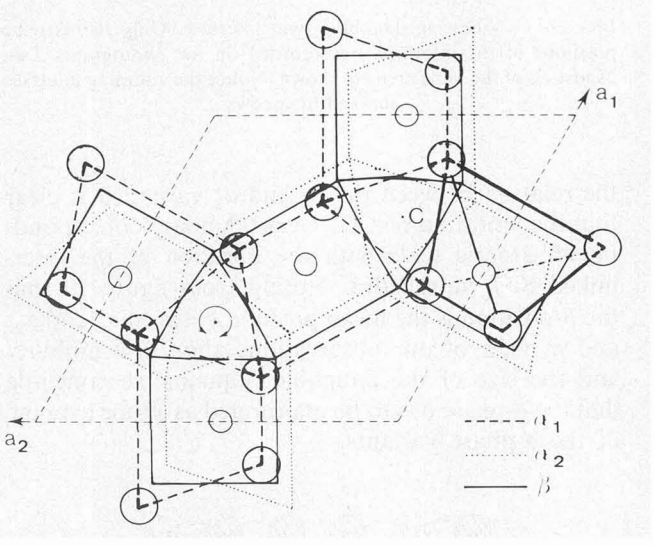

FIG. 19. — Schematic representation of the quartz structure. The two variants α_1 and α_2 of the low temperature phase as well as the β-phase are represented.

very mobile at temperatures just below the transition. In bright field images these defects are hardly visible, whereas a pronounced dark-light contrast is observed in the dark field images of particular reflections such as e.g. the $(30\bar{3}1)$ reflection in figure 20. These features together with the observation of only two variants allow us to identify these defects as the dauphiné twins described above, and the contrast as structure factor contrast. Indeed the extinction distances (structure factors) for some reflections which are simultaneously excited in the two crystal parts are drastically different e.g. for $30\bar{3}1$ $t_{\alpha_1} = 6\,049$ Å $t_{\alpha_2} = 1\,437$ Å.

A typical configuration of defects in a specimen at transition temperature where a temperature gradient of a few degrees is produced by the electron beam, was shown in figure 7. It was furthermore observed that the walls of the columnar domains of dauphiné twins are constantly vibrating. The closer to the transition the smaller the mesh size of the regular network of domains untill they reach sizes below the resolution limit of the microscope which is about 20 Å under these experimental conditions. Reminding

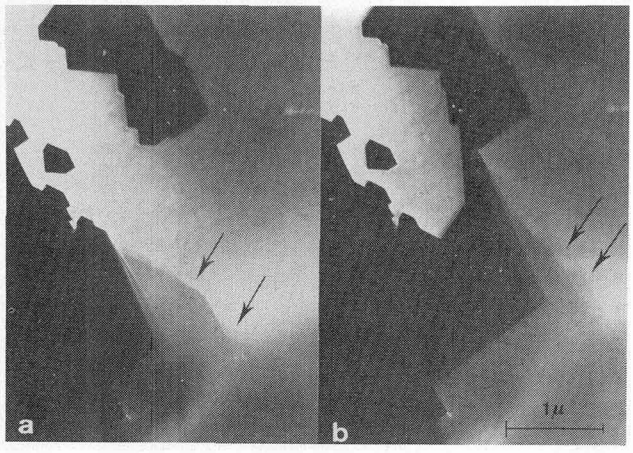

FIG. 20. — Vibrating dauphiné twin interface. Only the extreme positions of the interface are recorded on the photograph. Two exposures of the same area are shown. Notice the vibrating interface marked by arrows.

the relation between the α_1 and α_2 variant it is clear that the vibration of a D. Twin boundary corresponds on an atomic scale with the libration of the interlinked SiO_4 tetrahedra. Noting from figure 19 that the β-position is the mean position between α_1 and α_2, and in view of our observations about the mobility and the size of the dauphiné domains we conclude that the β-phase has to be interpreted as a time average of the α-phase variants.

3.3 ORDER-DISORDER TRANSITIONS IN β-In_2S_3 [15]. — β-In_2S_3 has a defective spinel structure containing octahedral as well as tetrahedral vacancies with respect to the normal spinel structure. The vacancies are ordered and from structural considerations different types of defects can be predicted. This structure analysis together with a study by electron microscopy and diffraction enabled to make a distinction between the defects associated with the tetrahedral vacancies and those with octahedral vacancies.

3.3.1 *Structural data.* — Described with respect to the close packed lattice of sulfur ions, the β-In_2S_3 structure can be considered as a stacking of two types of $(111)_S$ double layers (the index S in symbols of the type $(hkl)_S$ indicates that the indices are referred to the cubic spinel structure). The unit cell of β-In_2S_3 is in fact tetragonal with $c/a = 3$). Doublet layers containing octahedral ions only (figure 21, I) alternate with mixed doublet layers (figure 21, II) containing octahedral as well as tetrahedral cations. It is clear that both types of layers contain ordered arrays of vacancies. The nucleation of ordering in different areas of the continuous sulfur lattice at non-equivalent sites may thus give rise to ordering defects.

3.3.2 *Defects associated with order of the tetrahedral vacancies.* — Let us first consider the defects resulting from irregularities in the ordering of tetrahedral vacancies. Two types of two dimensional defects are expected :

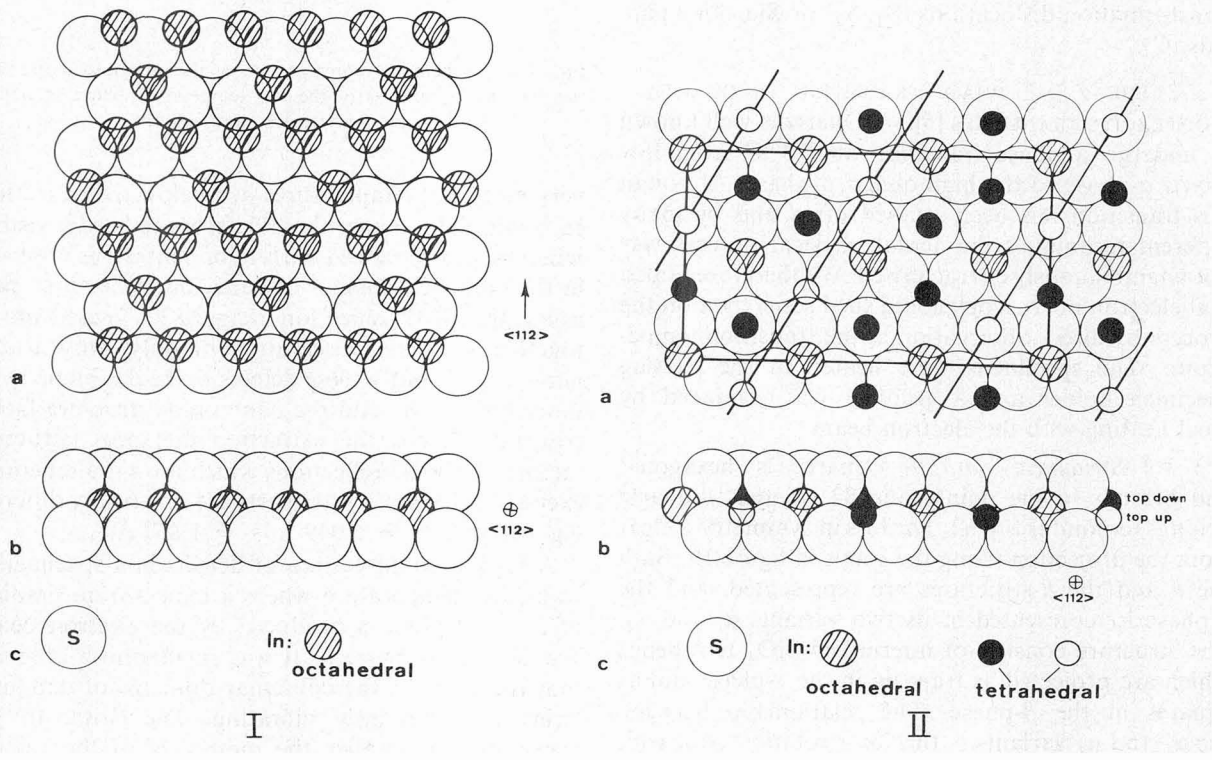

FIG. 21. — Structure of lamella occurring in β-In_2S_3. (I) Pure octahedral layer. (II) Mixed layer containing indium ions in octahedral as well as tetrahedral coordination.

3.3.2.1 *Antiphase boundaries* (*translation variants*). — If in the two parts of the continuous sulfur lattice the ordering has started at non-equivalent sites, causing the rows of vacancies indicated by full lines in figure 21I to be shifted with respect to each other, antiphase boundaries result. These antiphase boundaries can move laterally by means of correlated jumps of indium cations into neighbouring vacant sites. The arrows of figure 22*a* indicate e.g., the jumps required to move the boundary over a distance and in a direction given by $1/4\ a[11\bar{2}]_S$.

3.3.2.2 *Ordering twins* (*orientation variants*). — If the rows of tetrahedral vacancies enclose an angle of 120° or 60° ordering twins result with the $(110)_S$ plane as a coherent contact plane (figure 22*b*).

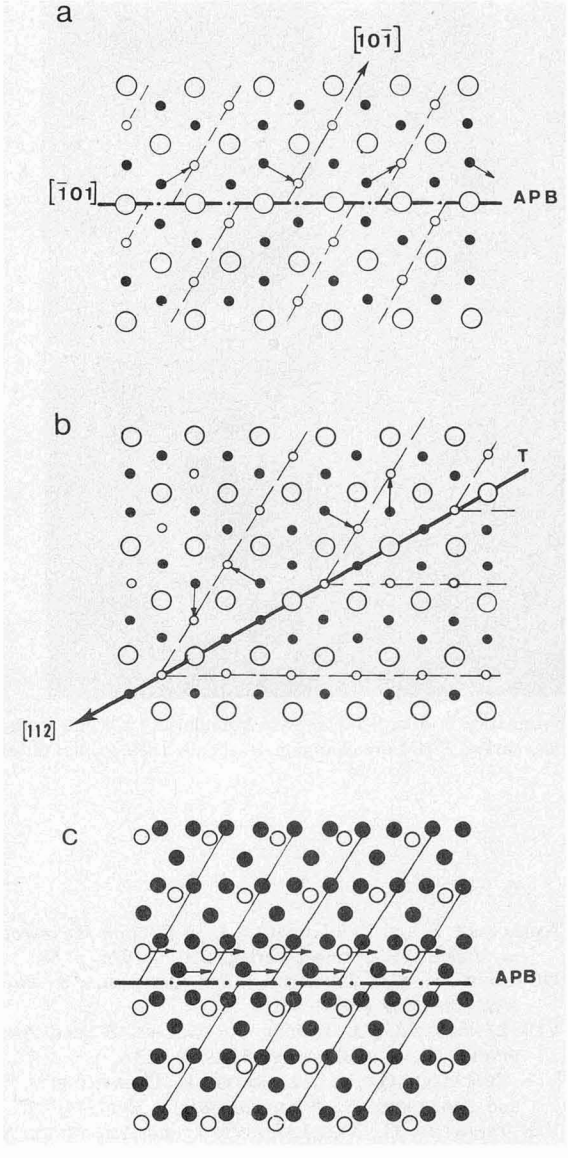

FIG. 22. — (*a*) Antiphase boundaries due to the wrong stacking of the tetrahedral indium ions. The arrows indicate the jumps required for movement of the boundary. (*b*) Twins associated with the wrong stacking of tetrahedral indium ions. (*c*) Antiphase boundaries associated with the wrong stacking of octahedral indium ions.

Again the boundaries are able to move laterally as a consequence of correlated jumps of the tetrahedral cations.

The jumps marked by an arrow on the figure will cause a lateral shift given by $3/4\ a[01\bar{1}]_S$.

3.3.3 *Defects associated with order in the octahedral vacancies.* — Upon inspection of figure 21, I, it is evident that due to the partial filling of the octahedral sites, antiphases boundaries are also possible as a consequence of mistakes in the filling of this type of sites. Figure 22*c* gives an example where for clarity reasons the sulfur ions and the tetrahedral indium cations have been omitted. It is important to notice that because of the symmetry of the arrangement of the octahedral interstices in both types of layers ordering twins are *not* expected from mistakes in the filling of these sites.

3.3.4 *Observations.* — Transmission electron microscopy of thin flakes of Czochralski grown β-In_2S_3 single crystals revealed different types of two-dimensional defects. These could be identified as antiphase boundaries and twin boundaries on the basis of contrast experiments. Figure 23 shows a typical area where both types of defects are observed.

By means of heating experiments it was also possible to make a distinction between the defects associated with the tetrahedral vacancies and those associated with the octahedral ones. It was observed that at a well-defined temperature one kind of antiphase boundary and simultaneously the twin boundaries become mobile, while another type of antiphase boundary remained remarkably stable. From these observations and the structure analysis we can conclude that the mobile defects are the antiphase boundaries and twins

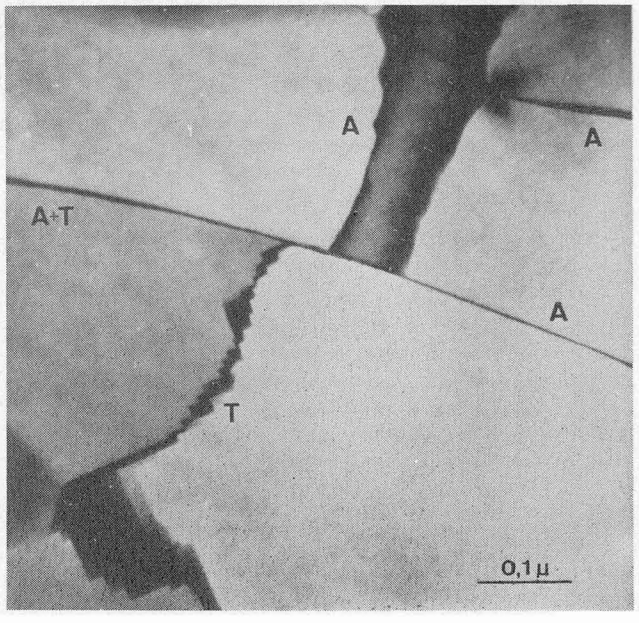

FIG. 23. — Ordering antiphase boundaries (A) and twins (T) in β-In_2S_3. The twin boundaries (T) consist of segments with a well-defined crystallographic orientation.

associated with the tetrahedral sublattice ; the stable boundaries are associated with the octahedral interstices. A heating sequence illustrating this behaviour is shown in figure 24.

If it is assumed that the movement of the defects constitute the onset of the disordering processes of indium ions in the two types of interstices, these observations together with the analysis of the structure model allow to propose a mechanism for the two transitions reported by Hatwell [16]. Since only the ordering of tetrahedral cations can cause two types of defects to become mobile simultaneously and since this occurs chronologically first in a heating experiment it is logical to associate it with the first transition at 420 °C.

The second transition at 750 °C is probably associated with the disordering of the cations in octahedral sites. The evidence for this last hypothesis is somewhat indirect but the observations of the antiphase boundaries associated with the octahedral cation arrangement do support this mechanism.

This example illustrates in particular the usefulness of the recognition and analysis of static ordering defects for obtaining information about the ordering mechanism.

Acknowledgments. — The author gratefully acknowledges Prof. S. Amelinckx for reading the manuscript and Dr. Van Tendeloo for the use of some photographs.

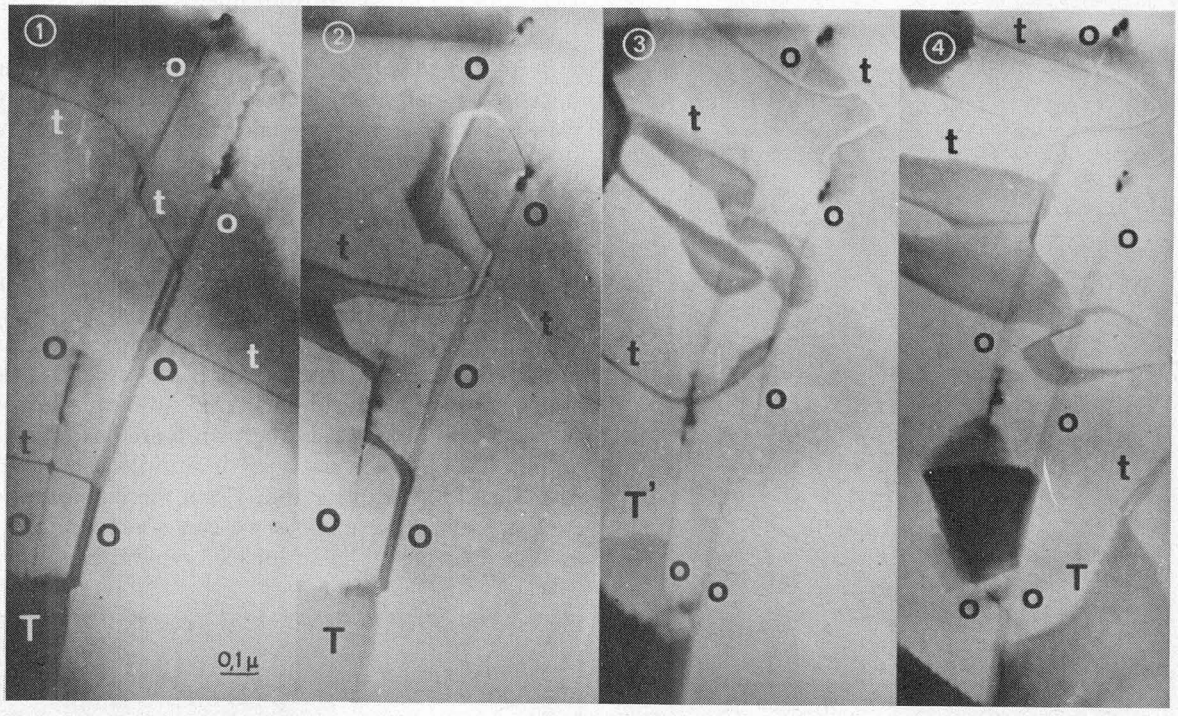

FIG. 24. — Heating sequence showing twins and two kinds of antiphase boundaries in β-In_2S_3. T = twin boundaries ; t = tetrahedral antiphase boundaries ; O = octahedral antiphase boundaries. The boundaries marked T en t are changing drastically their configuration.

References

[1] VAN LANDUYT, J., GEVERS, R. and AMELINCKX, S., *Phys. stat. sol.* **13** (1966) 467.

[2] DE RIDDER, R., VAN TENDELOO, G., VAN DYCK, D. and AMELINCKX, S., *Phys. stat. sol.* (a) **38** (1976) 663.

[3] VAN LANDUYT, J., *Phys. stat. sol.* **6** (1964) 957.

[4] VAN LANDUYT, J., VAN TENDELOO, G., AMELINCKX, S., *Phys. stat. sol.* (a) **36** (1976) 767.

[5] VAN TENDELOO, G., VAN LANDUYT, J., AMELINCKX, S., *Phys. stat. sol.* (a) **33** (1976) 732.

[6] VAN LANDUYT, J., VAN TENDELOO, G., AMELINCKX, S., *Phys. stat. sol.* (a) **26** (1974) 585.

[7] VAN LANDUYT, J., REMAUT, G. and AMELINCKX, S., *Phys. stat. sol.* **41** (1970) 271.

[8] VAN TENDELOO, G. and AMELINCKX, S., *Acta Crystallogr.* A **30** (1974) 431.

[9] AMELINCKX, S. and VAN LANDUYT, J., in *Electron Microscopy in Mineralogy* (Springer-Verlag, Berlin) 1976, p. 68.

[10] DE RIDDER, R., VAN LANDUYT, J. and AMELINCKX, S., *Phys. stat. sol.* (a) **9** (1972) 551.

[11] VAN LANDUYT, J., DE RIDDER, R., GEVERS, R. and AMELINCKX, S., *Mat. Res. Bull.* **5** (1970) 353.

[12] VAN TENDELOO, G., VAN LANDUYT, J., DELAVIGNETTE, P. and AMELINCKX, S., *Phys. stat. sol.* (a) **25** (1974) 697.

[13] VAN TENDELOO, G., VAN LANDUYT, J. and AMELINCKX, S., *Mat. Res. Bull.* **10** (1975) 941.

[14] MORTON, A. J., *Phys. stat. sol.* (a) **23** (1974) 275.

[15] VAN LANDUYT, J. and AMELINCKX, S., *Phys. stat. sol.* **31** (1969) 589.

[16] HATWELL, H., OFFERGELD, G., HERINCKX, C. and VAN CAKENBERGHE, J., *C. R. Hebd. Séan. Acad. Sci. C* **252** (1961) 3586.